Intrinsic scattering channels and selection rules in four-phonon interactions

Ying-Qin Lin,[1] Shu-Hao Cao,[1] Cui-E Hu,[2,*] Hua-Yun Geng,[3] and Xiang-Rong Chen[1,†]
[1]*Institute of Atomic and Molecular Physics, Sichuan University, Chengdu 610064, China*
[2]*College of Physics and Electronic Engineering, Chongqing Normal University, Chongqing 401331, China*
[3]*National Key Laboratory for Shock Wave and Detonation Physics Research, Institute of Fluid Physics, CAEP, Mianyang 621900, China*

(Received 9 May 2024; revised 2 July 2024; accepted 29 July 2024; published 9 August 2024)

We propose selection rules for four-phonon (4ph) scattering that clarify the predominance of the redistribution process. The cutoff frequencies for specific scattering channels are identified, with their feasibility determined by the magnitude of the *a*-*o* gap. We obtain substantive evidence to support the fact that the enhancement of 4ph scattering is due to the flat phonon dispersion. An extremely strong intraband scattering in the ZA branch is identified beyond expectation. The same enhancing effect can manifest between homothetic branches as an enhancement mechanism of interband scattering. The homothety is associated with the distribution trend of phonon group velocity, which can anticipate the intensity of 4ph scattering. Our work provides insights and perspectives into 4ph interaction.

DOI: 10.1103/PhysRevB.110.075414

I. INTRODUCTION

With growing demand for energy, lattice thermal conductivity (κ_l) is of intense interest in applications for energy recovery and renewable technologies, such as thermoelectricity [1–5], thermal barrier coating [6–8], and thermal management [9–12]. The three-phonon (3ph) scattering was considered to effectively describe the anharmonicity of κ_l in specific cases [13–15], with extensive studies in the associated selection rules. One such rule stipulates that two acoustic phonons cannot combine into an optical phonon when the *a*-*o* gap is sufficiently large [13]. In contrast, four-phonon (4ph) scattering is not subject to this constraint. The importance of 4ph scattering has been validated both theoretically and experimentally [16–18], but in what systems is the 4ph scattering particularly important? Previous studies showed that flat phonon dispersion can potentially amplify 4ph scattering [19]. In materials characterized by a large *a*-*o* gap and pronounced avoided crossing effects, 4ph scattering can be intense and dominate phonon-phonon (ph-ph) interactions, especially in low-κ_l systems [4,20,21]. These realizations have sparked interest in further investigating the mechanisms of 4ph scattering [22]. Extensive studies have been implemented across rattling guest atoms [23–25], self-consistent phonon theory [26–28], and phonon polariton [29–31]. However, the specific reasons why 4ph scattering is predominantly governed by the redistribution process remain elusive, with new mechanisms and selection rules anticipated. The correlation between flat dispersion and enhancement of 4ph scattering requests further validation, with the possibility of uncovering new physical behaviors.

In this paper, we choose Janus 2*H*-*M*SeTe (M = Zr, Hf) monolayers as an example to reveal the 4ph interaction. We here propose different selection rules for 4ph scattering. The permitting conditions and cutoff frequencies are clearly elucidated for the redistribution process. The *aooo*, *aaao*, and *aaoo* scattering involving acoustic (*a*) and optical (*o*) modes are examined to assess the influence of the *a*-*o* coupling. A different enhancement mechanism of interband scattering generated by homothetic phonon branches has been identified in accordance with the distribution trend of phonon group velocity.

II. THEORETICAL METHODS AND COMPUTATIONAL DETAILS

Our calculations were carried out by using the Vienna *ab initio* simulation package (VASP) [32,33] with the exchange-correlation function of Perdew, Burke, and Ernzerhof (PBE) [34]. The harmonic interatomic force constants (IFCs) are computed using the density functional perturbation theory (DFPT) method [23] in a 6 × 6 × 1 supercell. The third- and fourth-order IFCs are calculated using a 4 × 4 × 1 supercell and consider third-nearest and second-nearest neighbors, respectively. The ShengBTE and FourPhonon codes [35–37] were employed to estimate the lattice thermal conductivity involving 3ph and 4ph ($\kappa_l^{3,4ph}$) interactions with a 41 × 41 × 1 q mesh. The 4ph scattering rates (SRs) are expressed as [38]

$$\Gamma^{(++)}_{\lambda\lambda'\lambda''\lambda'''} = \frac{\hbar^2\pi}{8N}\frac{\left(1+n^0_{\lambda'}\right)\left(1+n^0_{\lambda''}\right)n^0_{\lambda'''}}{n^0_{\lambda}}\left|V^{(++)}_{\lambda\lambda'\lambda''\lambda'''}\right|^2 \times \frac{\delta(\omega_\lambda+\omega_{\lambda'}+\omega_{\lambda''}-\omega_{\lambda'''})}{\omega_\lambda\omega_{\lambda'}\omega_{\lambda''}\omega_{\lambda'''}}, \quad (1)$$

$$\Gamma^{(+-)}_{\lambda\lambda'\lambda''\lambda'''} = \frac{\hbar^2\pi}{8N}\frac{\left(1+n^0_{\lambda'}\right)n^0_{\lambda''}n^0_{\lambda'''}}{n^0_{\lambda}}\left|V^{(+-)}_{\lambda\lambda'\lambda''\lambda'''}\right|^2 \times \frac{\delta(\omega_\lambda+\omega_{\lambda'}-\omega_{\lambda''}-\omega_{\lambda'''})}{\omega_\lambda\omega_{\lambda'}\omega_{\lambda''}\omega_{\lambda'''}}, \quad (2)$$

*Contact author: cuiehu@cqnu.edu.cn
†Contact author: xrchen@scu.edu.cn

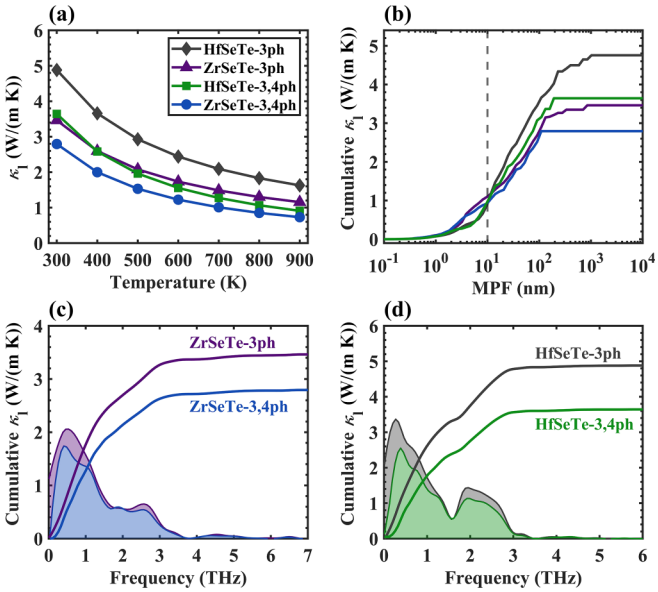

FIG. 1. (a) The κ_l of 3ph and 4ph from 300 to 900 K. (b) The cumulative κ_l as a function of MFP at 300 K. (c),(d) The κ_l contribution spectrum (the filled area below the lines) and cumulative κ_l as a function of frequency at 300 K for ZrSeTe and HfSeTe monolayers.

$$\Gamma^{(--)}_{\lambda\lambda'\lambda''\lambda'''} = \frac{\hbar^2\pi}{8N}\frac{n^0_{\lambda'}n^0_{\lambda''}n^0_{\lambda'''}}{n^0_{\lambda}}|V^{(--)}_{\lambda\lambda'\lambda''\lambda'''}|^2 \times \frac{\delta(\omega_\lambda - \omega_{\lambda'} - \omega_{\lambda''} - \omega_{\lambda'''})}{\omega_\lambda\omega_{\lambda'}\omega_{\lambda''}\omega_{\lambda'''}}, \quad (3)$$

where ω_λ is the phonon frequency, n_λ is the phonon Bose-Einstein distribution, and V is the transition probability matrices. The superscripts of $(++)$, $(+-)$, and $(--)$ are the notations of combination ($\lambda + \lambda' + \lambda'' \rightarrow \lambda'''$), redistribution ($\lambda + \lambda' \rightarrow \lambda'' + \lambda'''$), and splitting ($\lambda \rightarrow \lambda' + \lambda'' + \lambda'''$) processes in 4ph scattering, respectively.

III. RESULTS AND DISCUSSION

A. Lattice thermal conductivity for Janus 2*H*-*M*SeTe

The optimized lattice constants of ZrSeTe and HfSeTe monolayers are 3.87 and 3.85 Å, respectively, with the $P3m1$ space group in hexagonal structures. It is found from our results that, at 300 K, the κ_l^{3ph} are 3.46 and 4.88 W m^{-1} K^{-1}, and the $\kappa_l^{3,4ph}$ are 2.79 and 3.64 W m^{-1} K^{-1} for ZrSeTe and HfSeTe monolayers, respectively; at 900 K, the κ_l^{3ph} reduce to 1.16 and 1.63 W m^{-1} K^{-1}, while the $\kappa_l^{3,4ph}$ reduce to 0.73 and 0.91 W m^{-1} K^{-1}, respectively. It is worth noting that the κ_l for ZrSeTe and HfSeTe monolayers decreased markedly by 19.31% (36.74%) and 25.36% (44.07%) at 300 K (900 K) when considering the 4ph scattering. Crystals have more intensely anharmonic lattice vibrations at high temperatures, leading to a higher decreasing ratio in κ_l. Apparently, the impact of 4ph scattering on the κ_l is important and non-negligible. Figures 1(b)–1(d) illustrate the cumulative κ_l^{3ph} and $\kappa_l^{3,4ph}$ as functions of the phonon mean free path (MFP) and frequency, which reveal that phonons are greatly influenced by 4ph interactions. As shown in Fig. 1(b), $\kappa_l^{3,4ph}$ is suppressed, and the increasing rate markedly declines when MFP is greater than 10 nm. Compared to κ_l^{3ph}, $\kappa_l^{3,4ph}$ of ZrSeTe and HfSeTe rapidly converges near 100 nm.

As shown in Figs. 1(c) and 1(d), the majority contribution to the κ_l is concentrated below 3 THz, corresponding to the acoustic modes and low-frequency optical modes. In particular, the proportional contributions of out-of-plane (ZA) mode are 5.17% and 7.10% to $\kappa_l^{3,4ph}$ at 300 K for ZrSeTe and HfSeTe monolayers, respectively. Comparing 3ph and 4ph SRs, the relative intensity of the 4ph scattering and the effect on κ_l can be estimated. The 4ph SR is an order of magnitude smaller than 3ph SRs in Figs. 2(a) and 2(b) that illustrate the importance of 4ph scattering. For ZrSeTe and HfSeTe, the distribution of 4ph SRs is similar, and both show considerable scattering in the ZA mode at 0–1 THz. In Fig. 2(c), we separately compare the 4ph SRs of acoustic modes. The HfSeTe monolayer has higher SRs at 2–3 THz. After considering 4ph scattering, the decrease of κ_l within this range is more significant compared to ZrSeTe.

As shown in Figs. 3(a) and 3(b), the redistribution process with high SRs is predominant in 4ph scattering and induces a decreasing κ_l. It is approximately an order of magnitude larger than the splitting and combination processes. The scattering phase space is the summation in quantities of the permitted scattering channels that conserve energy and quasimomentum [14,39,40], which only depends on the characteristics of phonon dispersion. It is effective to analyze the effect of phonon dispersion characteristics on ph-ph interaction with phase space. In Figs. 3(c)–3(f), a high phase space of redistribution process is comparable to 3ph scattering. The total number of scattering channels in the redistribution process is also one order of magnitude higher than that in splitting and combination processes. The scattering can generally occur in reverse for combination and splitting processes, producing a symmetric phase space distribution that predominates in the low- and high-frequency regions, respectively. This distribution without uniformity is attributed to the absence of quantum states to accept the emitted phonons beyond the appropriate frequency regions [41,42]. Notably, the phase space of redistribution process is characterized by a flat distribution in Figs. 3(e) and 3(f), revealing an even distribution of scattering channels across the entire frequency region. Thus, it involves the scattering of all phonon branches. We contend that the dominance of the redistribution process is not accidental but rather an intrinsic mechanism in 4ph scattering.

B. Selection rules in four-phonon scattering

The available studies on the selection rules of 3ph scattering have already been comprehensive [13,40,43,44]. The 4ph scattering is concerned as a less restricted process by selection rules, which is more prone to conserve energy compared to 3ph scattering [43,45]. The selection rule is straightforward for splitting and combination processes. In phonon dispersion, each phonon branch has distinct upper and lower energy limits where the transition can be anticipated. Consider the 4ph combination process, assuming that the involved absorbed phonons derive from different branches. The sum of the maximum and minimum frequency values for these branches is

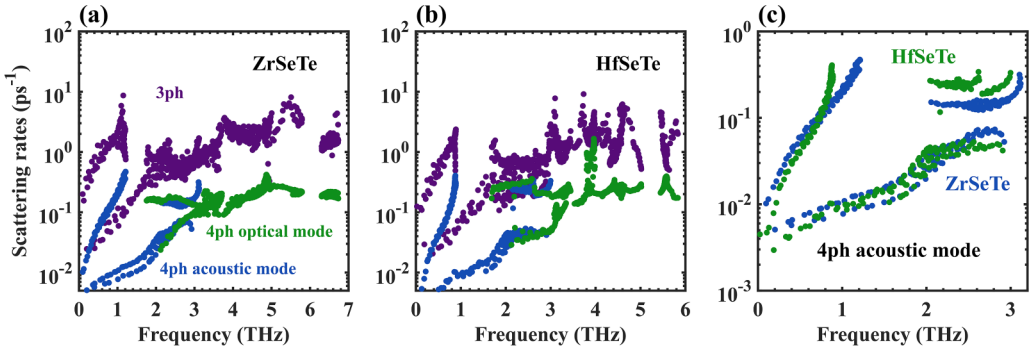

FIG. 2. (a),(b) The anharmonic 3ph and 4ph scattering rates at 300 K. (c) The acoustic modes of 4ph interaction for ZrSeTe and HfSeTe monolayers.

denoted as $\omega_{\max}$ and $\omega_{\min}$, respectively. Apparently, the branch accepting the emitted phonon must lie between $\omega_{\max}$ and $\omega_{\min}$. This can serve as a universal rule of energy for any phonon branch.

Selection rules for redistribution process. The features of phonon dispersion activate specific selection rules. To our knowledge, the 4ph selection rules have not been explicitly formulated. For the redistribution process, the conservation of energy can be reformulated into a more comprehensible form:

$$\omega(\lambda) + [\omega(\lambda) + \Delta\omega(\lambda', \lambda)] = [\omega(\lambda) + \Delta\omega(\lambda'', \lambda)] + [\omega(\lambda) + \Delta\omega(\lambda', \lambda) - \Delta\omega(\lambda', \lambda''')], \quad (4)$$

where $\omega(\lambda)$ is the phonon frequency; each term with the square brackets in Eq. (4) represents the phonon frequencies $\omega(\lambda')$, $\omega(\lambda'')$, and $\omega(\lambda''')$, respectively, and $\Delta\omega$ is the difference value between two phonons. Equation (4) is simplified as $\Delta\omega(\lambda'', \lambda) = \Delta\omega(\lambda', \lambda''')$ with a diagram depicted in Fig. 4. Notably, the frequency difference between λ''' and λ'' phonons will not affect the conservation of energy for the redistribution process. When the *a-o* gap lies between them, the *a-o* gap can be of any magnitude. Thus it can be deduced that, apart from the frequency difference between the participating phonons, there are no further restrictions on the upper and lower limits of phonon frequencies. As a result, the redistribution process can occur in each mode and cross an arbitrary width of the

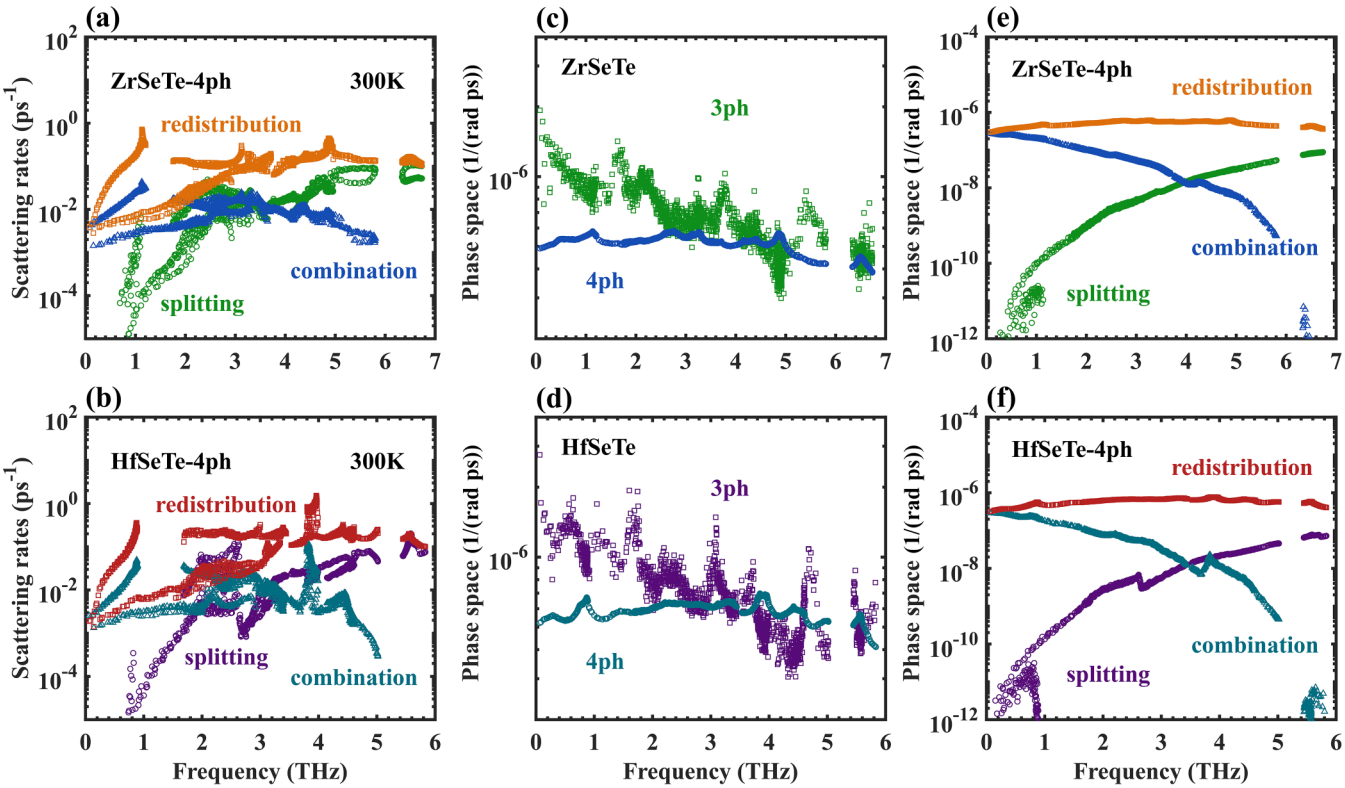

FIG. 3. (a),(b) The decomposed 4ph SRs into the splitting, redistribution, and combination processes at 300 K, (c),(d) the comparison of phase space in 3ph and 4ph interactions, and (e),(f) the decomposed phase space in 4ph scattering for ZrSeTe and HfSeTe monolayers.

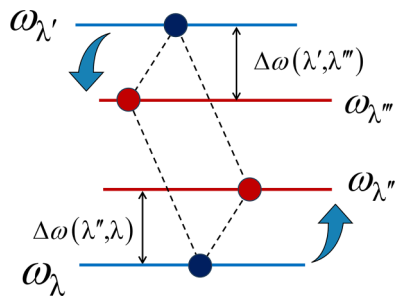

FIG. 4. A diagram for the redistribution process that conserves the energy and quasimomentum. The blue and red circles represent the absorbed and emitted phonons involved in this process, respectively.

a-o gap [43,46]. Even with a sufficiently large *a-o* gap, potentially prohibiting the splitting and combination processes across it, the redistribution process would not be hindered from occurring.

Now, we discuss the scattering channels in the redistribution process. The *aaaa*, *aoao*, and *oooo* scattering are universally present and typically dominate in the redistribution process, while *aooo*, *aaaa*, and *aaoo* only arise in specific cases.

(1) *aooo selection rule*. The *aooo* ($a + o \leftrightarrow o + o$) scattering is permitted when the bandwidth of optical modes ($\Delta\omega_{\mathrm{o}}$) is larger than the frequency range of *a-o* gap ($\Delta\omega_{\mathrm{a-o}}$), expressed as $\Delta\omega_{\mathrm{o}} \geqslant \Delta\omega_{\mathrm{a-o}}$. The selection rule establishes a cutoff frequency to conserve energy. The acoustic phonons below $\Delta\omega_{\mathrm{a}} - \Delta\omega_{\mathrm{o}} + \Delta\omega_{\mathrm{a-o}}$ are excluded from this process, where $\Delta\omega_{\mathrm{a}}$ represents the bandwidth of acoustic modes.

(2) *aaao selection rule*. The *aaao* ($a + a \leftrightarrow a + o$) scattering occurs when $\Delta\omega_{\mathrm{a}} \geqslant \Delta\omega_{\mathrm{a-o}}$ is satisfied. Considering an ideal situation, when participating acoustic phonons lie at the top or bottom of the acoustic region, the maximum of $\Delta\omega(\lambda'', \lambda)$ and $\Delta\omega(\lambda', \lambda''')$ must be less than $\Delta\omega_{\mathrm{a}}$. Thus, the maximal frequency window in optical phonons is $2\Delta\omega_{\mathrm{a}}$. It is noted that both *aooo* and *aaao* scattering only exist in materials with a small or nonexistent *a-o* gap.

(3) *aaoo selection rule*. The *aaoo* ($a + a \leftrightarrow o + o$) scattering occurs in materials without an *a-o* gap due to the inevitable intersection of *a-o* branches and requires $\Delta\omega_{\mathrm{a}} \geqslant 2\Delta\omega(\lambda'', \lambda)$. This activates an additional scattering channel and lies in proximity to the frequencies where *a-o* modes overlap. As with the *aaao* scattering, the optical phonons with frequencies exceeding $2\Delta\omega_{\mathrm{a}}$ cannot participate in this scattering process. For Janus 2*H*-*M*SeTe, the summing SRs of *aooo*, *aaao*, and *aaoo* are one order of magnitude smaller than those of redistribution process, implying their non-negligible effect.

As the *a-o* gap expands, the *aooo*, *aaao*, and *aaoo* scattering are suppressed or completely forbidden because conservation of energy becomes more challenging [47]. In contrast, these channels are particularly essential in materials with intense 4ph scattering or a small *a-o* gap, as well as in softened phonon dispersion and low-κ_{l} systems due to superior anharmonicity [14,21,48]. Hence, they can serve as quantifiable symbols to assess the substantive influence of an *a-o* gap and *a-o* coupling effect on the redistribution process. Our finding provides theoretical support for modulating the *a-o* gap to artificially control the thermal transport properties of materials [49–51]. In fact, the redistribution process facilitates interband scattering between low- and high-frequency modes, enabling their extension across arbitrary frequency intervals. This corresponds to a vast phase space that effectively compensates for the absence of frequency regions in other scattering processes. These explains the indispensable role of redistribution process.

C. Phonon interband and intraband scattering

Interband scattering can be categorized into multiple interband (MIS) and dual interband (DIS) scattering. Figures 5(a)–5(c) illustrate several potential instances of redistribution process in phonon dispersion, and the interband and intraband scattering are estimated for the ZrSeTe monolayer in Figs. 5(e) and 5(f). As shown in Figs. 5(a) and 5(b), the top of the out-of-plane (ZA) and longitudinal acoustic mode (LA) exhibits the characteristic of the localized flat dispersion in the ZrSeTe monolayer. The transverse acoustic branch (TA) has pronounced nonflatness and a larger frequency bandwidth. The DIS between specific branches allows a better assessment of the influence of flatness on SRs for redistribution process. The DIS between the out-of-plane optical branch ($\mathrm{ZO_1}$) branch with the ZA ($\mathrm{ZA} + \mathrm{ZO_1} \rightarrow \mathrm{ZA} + \mathrm{ZO_1}$), TA ($\mathrm{TA} + \mathrm{ZO_1} \rightarrow \mathrm{TA} + \mathrm{ZO_1}$), and LA ($\mathrm{LA} + \mathrm{ZO_1} \rightarrow \mathrm{LA} + \mathrm{ZO_1}$) branches can determine the effect of branch flatness on the SRs [Fig. 5(e)]. In the low-frequency region, the flatter ZA exhibits higher SRs than the TA and LA branches. There are several obvious peak values (dashed lines) of SRs in the channels involving TA and LA, coinciding precisely with the flat regions in phonon dispersion. The SRs of these three scattering channels are positively correlated with the flatness of phonon branches. Furthermore, the $\mathrm{ZO_1}$ branch shows relatively higher SRs approaching $10^{-1}\,\mathrm{ps}^{-1}$ near 5 THz, corresponding to the flat section. At 5–6 THz, the $\mathrm{ZO_1}$ branch becomes quite dispersive, accompanied by a markedly decreasing SRs. Meanwhile, this phenomenon applies to all scattering channels at 5–6 THz, indicating that the prominent phonon dispersion leads to a decline in SRs and disrupts the channels. The same decrease is also observed in the SRs of HfSeTe monolayer near 4 THz. Reflected in the phase space, this results in the suppressed phase space in Figs. 3(c) and 3(d). These demonstrate that flat phonon branches effectively enhance the redistribution process, consistent with previous theoretical research [19].

As shown in Fig. 5(d), the results reveal that interband scattering plays a crucial role, with both scatterings being comparable to the total SRs of the redistribution process. The MIS also has a certain advantage over DIS. Notably, there are more available scattering channels for interband scattering between each mode, resulting in a much higher phase space than intraband. Therefore, there is no longer a fundamentally different scattering mechanism beyond both scatterings in higher-order ph-ph interactions.

The importance of intraband scattering is generally overlooked due to the significant suppression in other 3ph and 4ph scattering processes. However, the flat curves enhance intraband scattering for the redistribution process with localized higher SRs. The absorbed and emitted phonons in these curves naturally satisfy conservation of energy for intraband

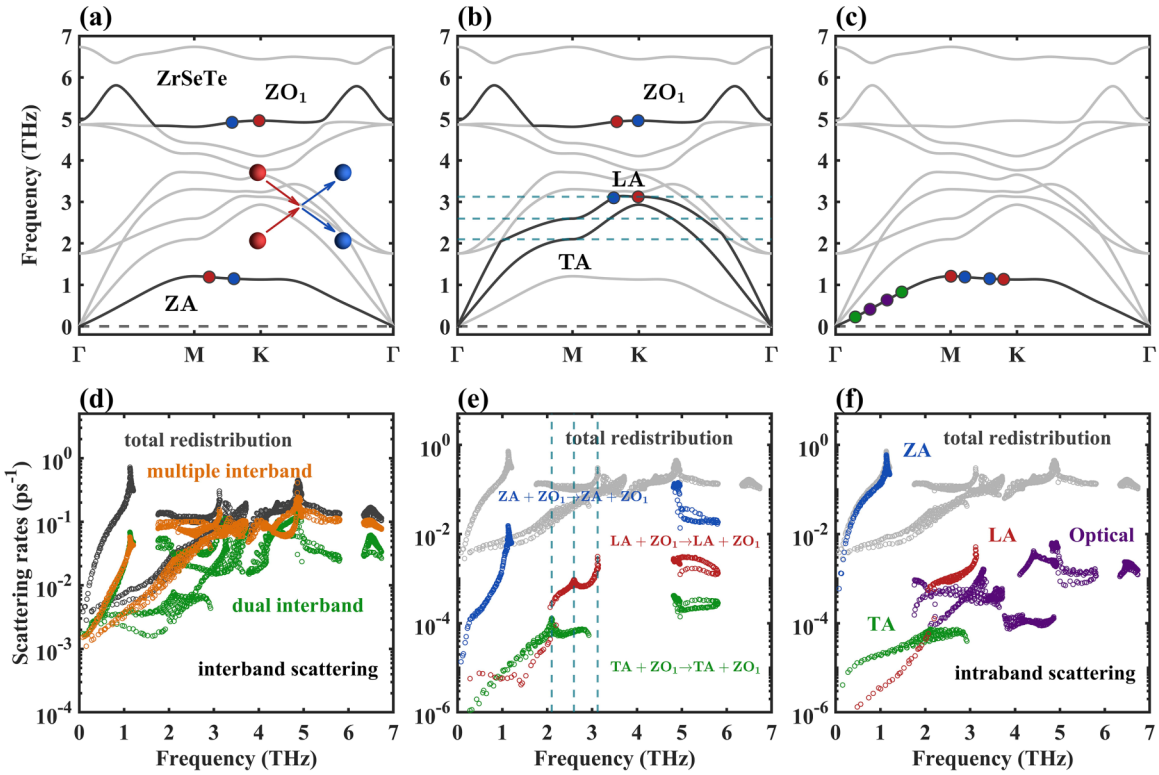

FIG. 5. (a)–(c) The possible DIS and intraband scattering in redistribution process. (d) The SRs of MIS and DIS. (e) The DIS between ZO_1 with ZA, TA, and LA branches. (f) The DIS for ZA, TA, LA, and optical modes at 300 K for ZrSeTe monolayer.

scattering. Interestingly, Fig. 5(f) shows that the ZA branch presents a strong intraband scattering for Janus 2*H*-*M*SeTe, which appears to be more intense than previously anticipated [52], thereby leading to a minimal contribution to κ_l. On the one hand, the pronounced linear (near the Γ point) and flat distribution provide abundant scattering channels cause the great SRs [53]. On the other hand, ZrSeTe and HfSeTe monolayers exhibit strong 3ph and 4ph scattering in the ZA branches attributed to their broken centrosymmetry, which allows for the scattering of odd and even out-of-plane modes, as per the symmetry selection rule [45,54,55]. In 1*T* and 2*H* phase monolayers with centrosymmetry, the 4ph interactions induce a dramatic increase in the SRs of ZA mode by evading the symmetry selection rules [56–58]. Hence, the importance of intraband scattering to the ZA branch can be basically confirmed in 4ph scattering, emphasizing its potential in other 2D systems.

D. Enhancement mechanism of interband scattering

The enhancement mechanism of flat phonon dispersion to the redistribution process can be extended to localized homothetic modes. Phonon branches with homothetic shapes are characterized by approximate distributions in absolute values of slope, which factually have the same physical fundamental as the phonon group velocity (v_g), i.e., $v_g = \partial\omega/\partial q$. The frequency relationship of the four phonons involved in the redistribution process can be expressed as follows:

$$\partial(\omega_\lambda + \omega_{\lambda'} - \omega_{\lambda''} - \omega_{\lambda'''})/\partial q = v_g + v'_g - v''_g - v'''_g = 0. \quad (5)$$

Apparently, energy conservation can be achieved when phonon group velocity has approaching values or a distribution trend. Excluding the influence of the flat mode and obtaining the scattering rates from homothetic branches pose a challenge, as the low SRs channels tend to be submerged. Helpfully, there is a clear correspondence between the peaks of high SRs. When more phonon branches exhibit localized homothety, it may generalize to the more universal MIS to be a novel enhancement mechanism of interband scattering.

To embody the homothety in ph-ph interactions, it is imperative to exclude the umklapp process in the following DIS. Figures 6(a) and 6(b) show the phonon dispersion and group velocities of TO_1, TO_2, ZO_1, and ZO_2 branches, and their DISs are depicted in Figs. 6(c) and 6(d). In phonon dispersion, the ZO_1 and ZO_2 branches are visually homothetic, with high SRs in $ZO_2 + ZO_1 \rightarrow ZO_2 + ZO_1$ at 4.37–4.61 and 5.44–5.60 THz (pink region) in Fig. 6(c), respectively. As shown in Fig. 6(d), there are identical SRs signatures for $TO_1 + ZO_1 \rightarrow TO_1 + ZO_1$ and $TO_1 + ZO_2 \rightarrow TO_1 + ZO_2$ that sufficiently demonstrate the homothety of ZO_1 and ZO_2. However, their distribution in group velocity seems different, which is less homothetic than ZO_1 and TO_2. The flat dispersed TO_2 branch gives rise to three significantly high SRs peaks in $ZO_2 + TO_2 \rightarrow ZO_2 + TO_2$. The low-lying SRs in this process attribute to the markedly dispersed TO_2 at 4.0–4.6 THz. Compared to ZO_2, $TO_2 + ZO_1 \rightarrow TO_2 + ZO_1$ has a high SR that implies its homothety in this region.

Furthermore, the group velocities show uniform distributions in the TO_1 and TO_2 branches, which are evidently different from other modes. They lack available phonon states in DIS that involve the ZO_2 branch. Notably, the

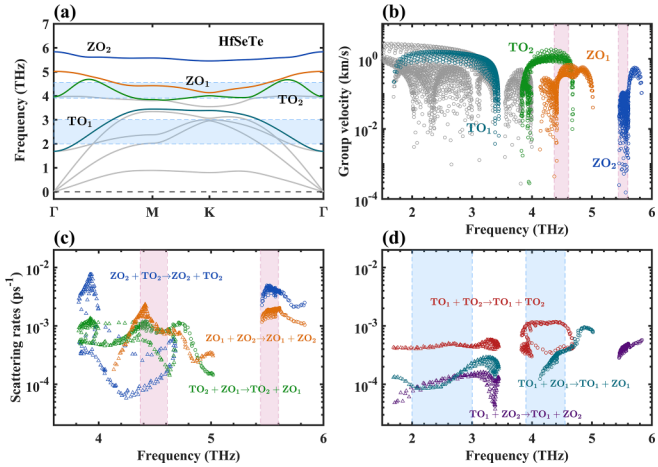

FIG. 6. (a) The TO_1, TO_2, ZO_1, and ZO_2 branches in the phonon dispersion for HfSeTe monolayer. (b) The group velocity for TO_1, TO_2, ZO_1, and ZO_2 branches. (c),(d) DIS of the normal process involves TO_1, TO_2, ZO_1, and ZO_2 branches in redistribution process at 300 K.

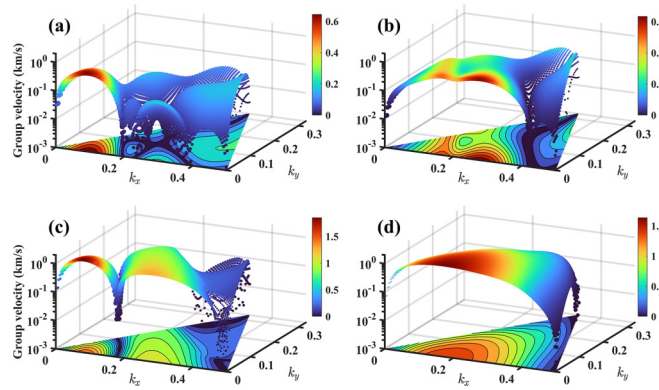

FIG. 7. The distribution of phonon group velocities and projected contour plots in the irreducible BZ for ZO_2 (a), ZO_1 (b), TO_2 (c), and TO_1 (d) branches, where the mark size reflects the magnitude of frequency.

$TO_1 + TO_2 \rightarrow TO_1 + TO_2$ scattering exhibits an unexpectedly higher SRs at 2–3 and 4.0–4.7 THz (blue region), implying the high SRs originate differently from flat modes. The linear dispersion in both TO_1 and TO_2 branches endows them with homothety while leading to their high SRs and uniformity in group velocities. The enhanced SRs arises from these validate our hypothesis.

Since the group velocity spectrum lacks information about quasimomentum, we further investigated group velocity distribution in the Brillouin zone (BZ) for ZO_2, ZO_1, TO_2, and TO_1 branches, as shown in Figs. 7(a)–7(d). The homothety between the ZO_1 and TO_2 branches is hardly reflected in the phonon dispersion but exhibits a flat distribution of phonon group velocity in the BZ, as shown in Figs. 7(b) and 7(c). Notably, the ZO_1 branch has a larger curvature compared to ZO_2 and an approximate bandwidth to TO_2 in phonon dispersion. This explains the comparable SRs of $TO_2 + ZO_1 \rightarrow TO_2 + ZO_1$ to $ZO_2 + TO_2 \rightarrow ZO_2 + TO_2$ channels. In fact, we find similar distribution characteristics between the ZO_2 and ZO_1 branches by comparing the projected contours in Figs. 7(a) and 7(b). The main distinction lies in the fact that ZO_2 presents more pronounced "valleys" in the group velocity. These valleys arise from extremum points with zero slope without diminishing ph-ph interactions. However, it does lead to a larger curvature in the group velocity distribution of ZO_2, which weakens the homothety to some extent. Hence, the DIS between ZO_2 and ZO_1 is not as pronounced as expected compared to flat modes. Moreover, disregarding the influence of group velocity valleys on the distribution trend to TO_2, the homothety between the TO_1 and TO_2 branches is undeniable in Figs. 7(c) and 7(d), with decreasing group velocities along the x axis.

IV. CONCLUSIONS

In summary, we discover different selection rules for 4ph scattering, which suggests that two pairs of participating phonons with equal frequency differences satisfy energy conservation. The occurring conditions and cutoff frequencies for *aooo*, *aaao*, and *aaoo* scattering channels are specified, enabling quantification of the influence of *a-o* coupling. The redistribution process establishes more available interband scattering channels, leading to its dominance in 4ph scattering and less constraint on energy conservation. By investigating DIS, we have confirmed the fact that flat phonon branches can enhance the 4ph interaction. Similarly, the localized homothetic branches exhibit the same behavior as the flat mode, characterized by the approximate distribution of phonon group velocities. This suggests a different enhancing mechanism for interband scattering. Our work confirms the importance of the redistribution process and provides insights and perspectives into 4ph interaction.

ACKNOWLEDGMENT

This work was supported by the National Natural Science Foundation of China (Grant No. 12074274).

[1] J. He and T. M. Tritt, Science **357**, eaak9997 (2017).
[2] C. Chen, Z. Feng, H. Yao, F. Cao, B. H. Lei, Y. Wang, Y. Chen, D. J. Singh, and Q. Zhang, Nat. Commun. **12**, 5718 (2021).
[3] B. Hinterleitner, I. Knapp, M. Poneder, Y. Shi, H. Müller, G. Eguchi, C. Eisenmenger-Sittner, M. Stöger-Pollach, Y. Kakefuda, N. Kawamoto *et al.*, Nature (London) **576**, 85 (2019).

[4] S. Han, S. Dai, J. Ma, Q. Ren, C. Hu, Z. Gao, M. D. Le, D. Sheptyakov, P. Miao, S. Torii *et al.*, Nat. Phys. **19**, 1649 (2023).

[5] L. D. Zhao, S. H. Lo, Y. Zhang, H. Sun, G. Tan, C. Uher, C. Wolverton, V. P. Dravid, and M. G. Kanatzidis, Nature (London) **508**, 373 (2014).

[6] N. P. Padture, Nat. Mater. **15**, 804 (2016).

[7] Z. Chen, Y. Wang, Y. Huang, F. Peng, C. Lin, W. Zheng, X. Song, Y. Niu, and Y. Zeng, npj Mater. Degrad **8**, 37 (2024).

[8] P. Zhang, E. Wang, X. Duan, X. Xie, D. Ding, T. Yang, Y. Zhao, and X. Hou, J. Alloys Compd. **952**, 169978 (2023).

[9] Y. Cui, Z. Qin, H. Wu, M. Li, and Y. Hu, Nat. Commun. **12**, 1284 (2021).

[10] X. Liu, W. Zhang, X. Zhang, Z. Zhou, C. Wang, Y. Pan, B. Hu, C. Liu, C. Pan and C. Shen, Nat. Commun. **15**, 3076 (2024).

[11] M. Zdrojek, Nature (London) **597**, 637 (2021).

[12] P. Xiao, A. El Sachat, E. C. Angel, R. C. Ng, G. Nikoulis, J. Kioseoglou, K. Termentzidis, C. M. S. Torres, and M. Sledzinska, Sci. Adv. **10**, eadm8825 (2024).

[13] L. Lindsay, D. A. Broido, and T. L. Reinecke, Phys. Rev. Lett. **111**, 025901 (2013).

[14] J. Ding, T. Lanigan-Atkins, M. Calderon-Cueva, A. Banerjee, D. L. Abernathy, A. Said, A. Zevalkink, and O. Delaire, Sci. Adv. **7**, abg1449 (2021).

[15] N. K. Ravichandran and D. Broido, Nat. Commun. **10**, 827 (2019).

[16] J. S. Kang, M. Li, H. Wu, H. Nguyen, and Y. Hu, Science **361**, 575 (2018).

[17] S. Li, Q. Zheng, Y. Lv, X. Liu, X. Wang, P. Y. Huang, D. G. Cahill, and B. Lv, Science **361**, 579 (2018).

[18] F. Tian, B. Song, X. Chen, N. K. Ravichandran, Y. Lv, K. Chen, S. Sullivan, J. Kim, Y. Zhou, T. H. Liu *et al.*, Science **361**, 582 (2018).

[19] L. Xie, J. H. Feng, R. Li, and J. Q. He, Phys. Rev. Lett. **125**, 245901 (2020).

[20] A. Kundu, X. Yang, J. Ma, T. Feng, J. Carrete, X. Ruan, G. K. H. Madsen, and W. Li, Phys. Rev. Lett. **126**, 115901 (2021).

[21] Y. Xia, K. Pal, J. He, V. Ozolins, and C. Wolverton, Phys. Rev. Lett. **124**, 065901 (2020).

[22] X. Qian, J. Zhou, and G. Chen, Nat. Mater. **20**, 1188 (2021).

[23] T. Tadano, Y. Gohda, and S. Tsuneyuki, Phys. Rev. Lett. **114**, 095501 (2015).

[24] T. Tadano and S. Tsuneyuki, Phys. Rev. Lett. **120**, 105901 (2018).

[25] J. Qi, B. Dong, Z. Zhang, Z. Zhang, Y. Chen, Q. Zhang, S. Danilkin, X. Chen, J. He, L. Fu *et al.*, Nat. Commun. **11**, 5197 (2020).

[26] K. Kim, W. Hwang, S.-H. V. Oh, and A. Soon, npj Comput. Mater. **9**, 154 (2023).

[27] T. Yue, Y. Zhao, J. Ni, S. Meng, and Z. Dai, npj Comput. Mater. **9**, 17 (2023).

[28] J. Zheng, C. Lin, C. Lin, G. Hautier, R. Guo, and B. Huang, npj Comput. Mater. **10**, 30 (2024).

[29] Y. Pei, L. Chen, W. Jeon, Z. Liu, and R. Chen, Nat. Commun. **14**, 8242 (2023).

[30] Z. Pan, G. Lu, X. Li, J. R. McBride, R. Juneja, M. Long, L. Lindsay, J. D. Caldwell, and D. Li, Nature (London) **623**, 307 (2023).

[31] Y. Wu, J. Ordonez-Miranda, S. Gluchko, R. Anufriev, D. S. Meneses, L. Del Campo, S. Volz, and M. Nomura, Sci. Adv. **6**, eabb4461 (2020).

[32] G. Kresse, J. Furthmüller, and J. Hafner, Europhys. Lett. **32**, 729 (1995).

[33] G. Kresse and J. Furthmüller, Phys. Rev. B **54**, 11169 (1996).

[34] J. P. Perdew, K. Burke, and M. Ernzerhof, Phys. Rev. Lett. **77**, 3865 (1996).

[35] W. Li, J. Carrete, N. A. Katcho, and N. Mingo, Comput. Phys. Commun. **185**, 1747 (2014).

[36] Z. Han, X. Yang, W. Li, T. Feng, and X. Ruan, Comput. Phys. Commun. **270**, 108179 (2022).

[37] L. Chaput, Phys. Rev. Lett. **110**, 265506 (2013).

[38] T. Feng and X. Ruan, Phys. Rev. B **93**, 045202 (2016).

[39] L. Lindsay and D. A. Broido, J. Phys.: Condens. Matter **20**, 165209 (2008).

[40] N. K. Ravichandran and D. Broido, Nat. Commun. **12**, 3473 (2021).

[41] G. Sun, J. Ma, C. Liu, Z. Xiang, D. Xu, T.-H. Liu, and X. Luo, Int. J. Heat Mass Transf. **215**, 124475 (2023).

[42] K. Ghosh, A. Kusiak, and J.-L. Battaglia, Phys. Rev. B **108**, 214309 (2023).

[43] N. K. Ravichandran and D. Broido, Phys. Rev. X **10**, 021063 (2020).

[44] S. Mukhopadhyay, L. Lindsay, and D. S. Parker, Phys. Rev. B **93**, 224301 (2016).

[45] Y. Han, C. Yang, X. Cheng, D. Han, W. Ding, and X. Wang, ACS Appl. Energy Mater. **7**, 649 (2023).

[46] X. Yang, T. Feng, J. Li, and X. Ruan, Phys. Rev. B **100**, 245203 (2019).

[47] S. Li, Z. Qin, H. Wu, M. Li, M. Kunz, A. Alatas, A. Kavner, and Y. Hu, Nature (London) **612**, 459 (2022).

[48] J. Klarbring, O. Hellman, I. A. Abrikosov, and S. I. Simak, Phys. Rev. Lett. **125**, 045701 (2020).

[49] H. Xiang and Y. Zhou, J. Eur. Ceram. Soc. **40**, 1352 (2020).

[50] H. Kim, G. Park, S. Park, and W. Kim, ACS Nano **15**, 2182 (2021).

[51] J. He, C. Yu, S. Lu, S. Shan, Z. Zhang, and J. Chen, Nanotechnology **35**, 025703 (2023).

[52] T. Feng and X. Ruan, Phys. Rev. B **97**, 045202 (2018).

[53] B. Peng, H. Zhang, H. Shao, Y. Xu, X. Zhang, and H. Zhu, Sci. Rep. **6**, 20225 (2016).

[54] C. Yu, Y. Hu, J. He, S. Lu, D. Li, and J. Chen, Appl. Phys. Lett. **120**, 132201 (2022).

[55] L. Lindsay, D. A. Broido, and N. Mingo, Phys. Rev. B **82**, 115427 (2010).

[56] Z. Tang, X. Wang, J. Li, C. He, M. Chen, C. Tang, and T. Ouyang, Phys. Rev. B **108**, 214304 (2023).

[57] H. Guo, W. Yan, J. Sun, Y. Pan, H. He, Y. Zhang, F. Yang, Y. Wang, C. Zhang, R. Li *et al.*, Mater. Today Phys. **40**, 101314 (2024).

[58] Y. Zhang, Z. Tong, A. Pecchia, C. Yam, T. Dumitrica, and T. Frauenheim, Nanoscale **14**, 13053 (2022).